

Establishing the Context for Reconnection Diffusion Region Encounters and Strategies for the Capture and Transmission of Diffusion Region Burst Data by MMS

T.D. Phan¹ · M.A. Shay² · J.P. Eastwood³ ·
V. Angelopoulos⁴ · M. Oieroset¹ · M. Oka¹ · M. Fujimoto⁵

Received: 16 October 2014 / Accepted: 2 April 2015 / Published online: 15 April 2015
© The Author(s) 2015. This article is published with open access at Springerlink.com

Abstract This paper describes the efforts of our Inter-Disciplinary Scientist (IDS) team to (a) establish the large-scale context for reconnection diffusion region encounters by MMS at the magnetopause and in the magnetotail, including the distinction between X-line and O-line encounters, that would help the identification of diffusion regions in spacecraft data, and (b) devise possible strategies that can be used by MMS to capture and transmit burst data associated with diffusion region candidates. At the magnetopause we suggest the strategy of transmitting burst data from all magnetopause crossings so that no magnetopause reconnection diffusion regions encountered by the spacecraft will be missed. The strategy is made possible by the MMS mass memory and downlink budget. In the magnetotail, it is estimated that MMS will be able to transmit burst data for all diffusion regions, all reconnection jet fronts (a.k.a. dipolarization fronts) and separatrix encounters, but less than 50 % of reconnection exhausts encountered by the spacecraft. We also discuss automated burst trigger schemes that could capture various reconnection-related phenomena. The identification of candidate diffusion region encounters by the burst trigger schemes will be verified and improved by a Scientist-In-The-Loop (SITL). With the knowledge of the properties of the region surrounding the diffusion region and the combination of automated burst triggers and further optimization by the SITL, MMS should be able to capture most diffusion regions it encounters.

Keywords Magnetospheric multiscale mission · Magnetic reconnection · Diffusion region · Burst triggers

✉ T.D. Phan
phan@ssl.berkeley.edu

¹ University of California, Berkeley, CA, USA

² University of Delaware, Newark, DE, USA

³ Imperial College, London, UK

⁴ University of California at Los Angeles, Los Angeles, CA, USA

⁵ ISAS, Sagamihara, Japan

1 Introduction

The primary objective of the MMS mission is to explore and understand the fundamental plasma physics of magnetic reconnection, with emphasis on kinetic plasma processes in the diffusion region that are responsible for collisionless reconnection (Burch et al. 2015, [this issue](#)). This objective is challenging experimentally because (1) highly accurate particle and field measurements must be made at extremely high sampling rates by four spacecraft and (2) the reconnection diffusion region is seldom encountered by spacecraft because of its minuscule scale size: the widths of the ion and electron diffusion regions perpendicular to the current sheet normal, which scale as the ion and electron inertial lengths, are of the order of 50 km and 1 km, respectively, at the magnetopause, and 2000 km and 50 km, respectively, in the magnetotail.

The success of the MMS mission thus depends critically on the optimization of the mission design so that the chance of diffusion region encounters is maximized. Furthermore, MMS must be able to capture particle and fields observations during each encounter with sufficient temporal resolution and accuracy so that the fundamental physical processes are revealed. To ensure success, it must be established during the mission design phase (1) where at the magnetopause and in the magnetotail one has the best chance of encountering the diffusion region, (2) how best to identify the ion and electron diffusion regions at the magnetopause and in the magnetotail, and (3) how best to evaluate, reduce and transmit burst data to the ground.

The MMS instrument capabilities are described in various chapters in this book, while the design of the MMS orbits to maximize the chance of diffusion region encounters is described by Fuselier et al. (2015, [this issue](#)). The present chapter describes the efforts by our Inter-Disciplinary Scientist (IDS) team to (a) establish the contexts for reconnection diffusion region encounters that would help the identification of diffusion regions in spacecraft data (Section 2), and (b) devise possible strategies for capturing and transmitting burst data of diffusion region candidates (Section 3).

2 Contexts for Diffusion Region Encounters

There are different approaches to determining whether a spacecraft has encountered the diffusion region or not. One approach is to identify the diffusion region based on theoretically expected kinetic signatures of diffusion region processes (e.g., Zenitani et al. 2012). The inter-comparison between theory and observations will be an important element in the analysis of MMS data to determine the key diffusion region processes. However, using such an approach alone to identify the diffusion regions could potentially bias the observations toward the existing theoretical models of reconnection, rather than gathering an unbiased sample of all the possible types of diffusion regions that may exist. An alternative or complementary approach is to identify diffusion region candidates by their large-scale context, e.g., the properties of the region surrounding the ion and electron diffusion regions. Such a scheme is likely to have a better chance of capturing an unbiased sample of diffusion regions, and provides consistency checks for the interpretation of diffusion region encounters based on observed and predicted kinetic signatures.

Another advantage with establishing the large-scale context is that, as will be described in Section 3, part of the procedure by which diffusion region candidates will be identified involves decisions made on the ground by a scientist-in-the-loop (SITL) in near real time based on transmitted low-resolution plasma and field survey data (Fuselier et al. 2015, [this issue](#)).

Such data does not have the required accuracy and resolution for examining the kinetic signatures of reconnection, but it should be adequate for establishing the large-scale contexts of diffusion region encounters. We now discuss the expected large-scale contexts for reconnection in magnetotail and magnetopause current sheets which have different boundary conditions in terms of inflow asymmetries as well as the size of the guide field (or magnetic shear angle). We will also discuss the distinction between X-line and O-line (i.e., flux rope) encounters.

2.1 Magnetotail

While technically it is possible for a spacecraft to encounter the diffusion region from any direction, a majority of the diffusion region encounters reported in the Near-Earth magnetotail have been associated with the tailward motion of an X-line past the spacecraft (e.g., Runov et al. 2003; Borg et al. 2005; Chen et al. 2008a; Eastwood et al. 2010a, 2010b), i.e. the spacecraft crossed the diffusion region along the outflow direction, observing both exhausts.

Near-Earth magnetotail reconnection involves essentially symmetric inflow plasma and field conditions with a small (<20 %) guide field. If a spacecraft flies through the ion diffusion region along the outflow direction, the expected large-scale signatures would be a reversal of plasma jetting, accompanied by a reversal of the normal component of the magnetic field. Coinciding with these reversals, one would also expect to detect portions of the quadrupolar out-of-plane Hall magnetic field (e.g., Oieroset et al. 2001; Runov et al. 2003; Borg et al. 2005; Eastwood et al. 2010a, 2010b) and bi-polar Hall electric field (Wygant et al. 2005; Borg et al. 2005; Eastwood et al. 2007). Figure 1 displays an example of reported ion diffusion crossing by the Cluster spacecraft (Borg et al. 2005) indicated by the reversals of the reconnection jets (Fig. 1(c)) and normal magnetic field (Fig. 1(h)). The out-of-plane magnetic field B_y pattern (Fig. 1(m)) is consistent with the predicted quadrupolar Hall field (Fig. 1(l)) (e.g., Sonnerup 1979), while the normal electric field E_z pattern (Fig. 1(n)), with $E_z < 0$ for $B_x > 0$ and $E_z > 0$ for $B_x < 0$, is consistent with the predicted converging Hall electric field structure (Fig. 1(l)) (e.g., Shay et al. 1998).

If a spacecraft encounters the neutral sheet (where the reconnecting field vanishes) during the flow reversal, it could indicate that the spacecraft is in the vicinity of the electron diffusion region. According to current theories of symmetric reconnection with small guide field (application to near-Earth magnetotail), the inner electron diffusion region is characterized by a large out-of-plane current centered around the electron jet reversal (e.g., Shay and Drake 1998; Hesse et al. 1999). The panels of Fig. 2 show an example of the expected flow signatures around the electron diffusion region in kinetic simulations. A horizontal cut through the diffusion region at the mid-plane ($z = 0$) shows ion and electron outflow jet reversals (panel b), as well as a large into-the-plane electron jet co-located with the jet reversals implying a strong out-of-plane current in the electron diffusion region.

Because the inner electron diffusion region is so small, there have been few reports of encounters with this region. Chen et al. (2008a), with guidance from kinetic simulations, reported the encounter by the Cluster spacecraft of a thin (electron-scale) current sheet in the vicinity of an X-line. More recently, Nagai et al. (2011, 2013) and Zenitani et al. (2012) reported a fortuitous encounter with the electron diffusion region in the Earth's magnetotail. In addition to observing the reversals of the ion and electron outflow velocity expected in the vicinity of the diffusion region, Geotail detected a strong into-the-plane electron jet right around the jet reversal, a key predicted characteristic of the inner electron diffusion region

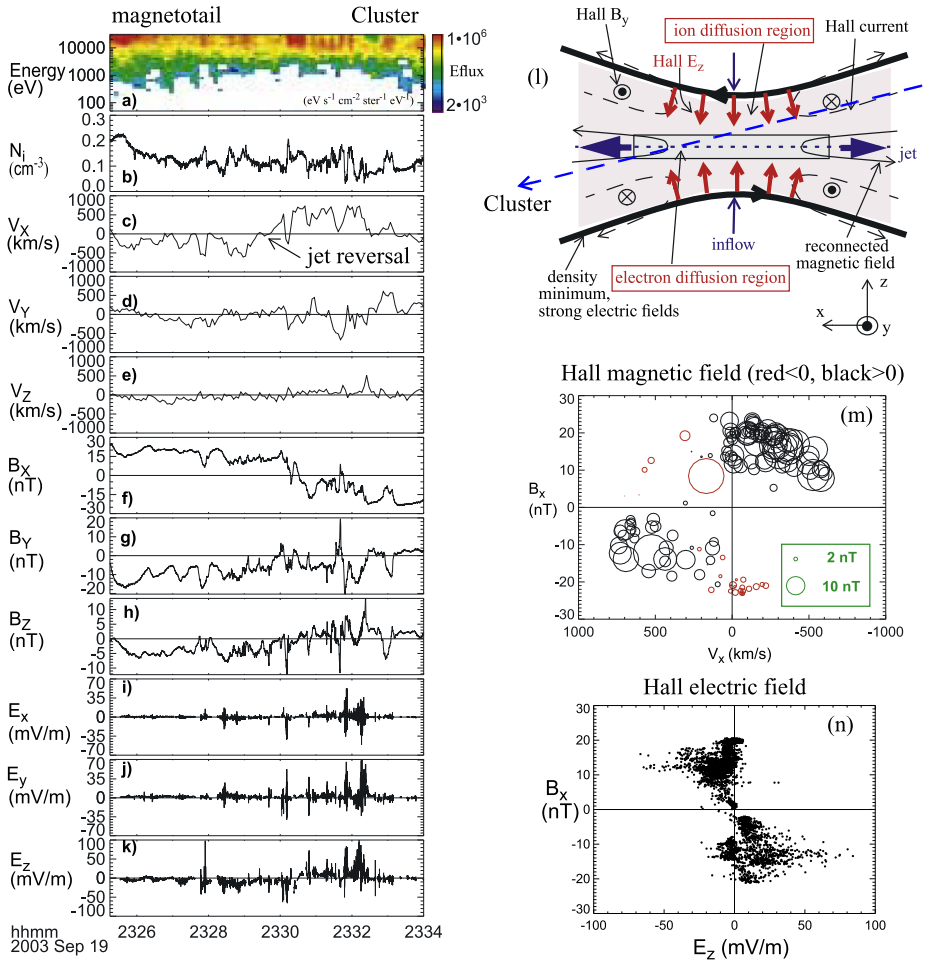


Fig. 1 Cluster spacecraft 4 crossing of the ion diffusion region in the near-Earth magnetotail on September 19, 2003. (a) Proton spectrogram; (b) density derived from spacecraft potential; (c)–(e) proton velocity (GSM); (f)–(h) magnetic field (GSM); (i)–(k) electric field (GSM); (l) the geometry of the magnetic reconnection diffusion region; (m) B_x versus v_x with B_y represented as circles for the interval plotted in the left panels. A black circle indicates a negative value of out-of-plane magnetic field B_y and a red circle a positive value, with the circle size being relative to the size of B_y ; (n) scatterplot of B_x versus E_z . Cluster was located at $(X, Y, Z)_{GSM} = (17.5, 3.4, 0.6)R_E$. Figure adapted from Borg et al. (2005)

(Shay and Drake 1998; Hesse et al. 1999). However, the temporal resolution of the Geotail plasma instrument was 12 seconds, thus only two particle distributions were collected by Geotail in the vicinity of the electron diffusion region. MMS will have much higher resolution measurements, and will be able to resolve the electron diffusion region in the magnetotail in much more detail.

It is more difficult to identify the electron diffusion region in cases where the spacecraft crossing is normal to the current sheet because no reversals of the outflow jets and normal field would occur that could help indicate the proximity of the spacecraft to the X-line. Furthermore, the Hall B_y and E_z (in GSM coordinates) extend some distance downstream of the ion diffusion region (e.g., Shay et al. 2007; Phan et al. 2007), thus their detection

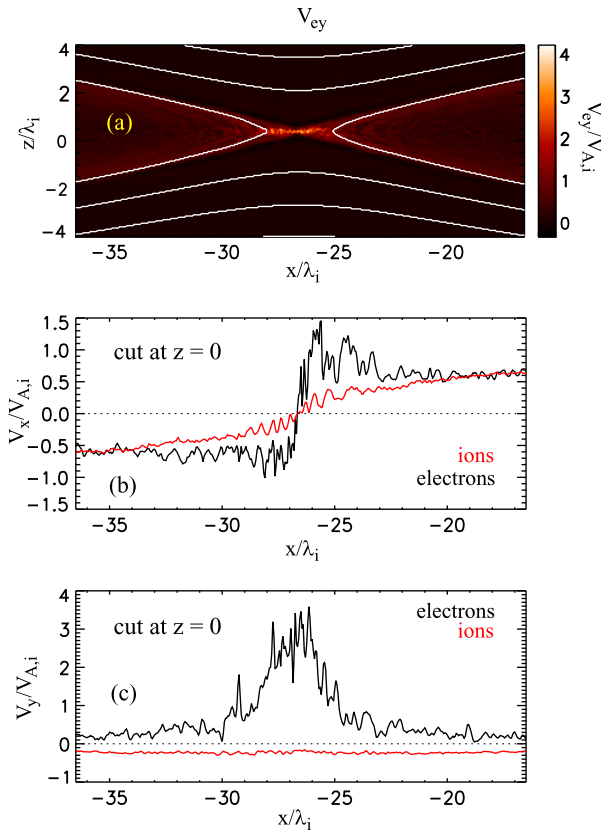
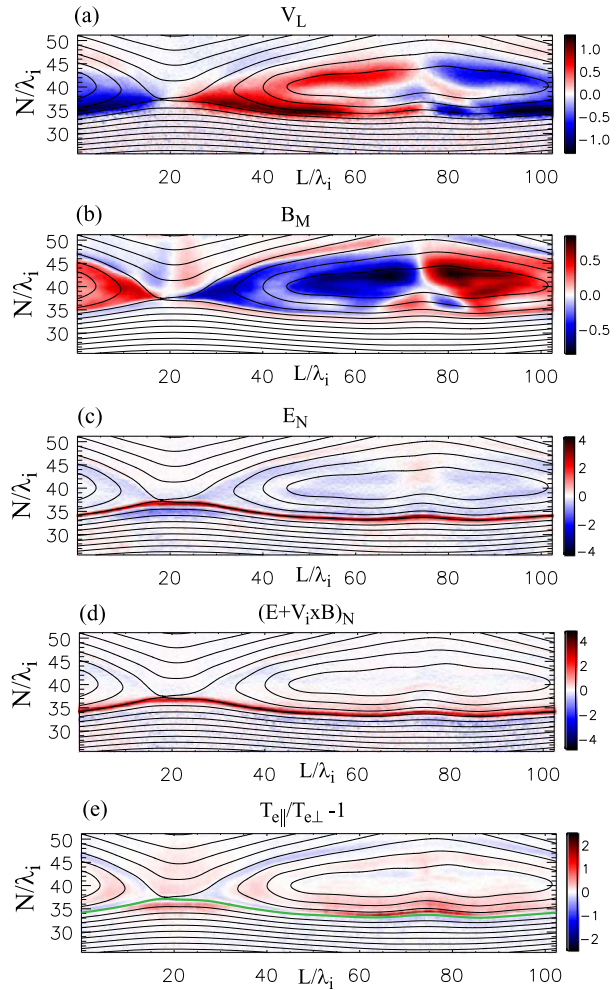


Fig. 2 Hybrid simulation of symmetric reconnection (particle ions and fluid electrons). **(a)** Electron out-of-plane flow with magnetic field lines. The electron diffusion region is associated with the intense electron flow at the center. **(b)** 1-D cuts along x at $z = 0$ of the electron and ion velocities in the outflow direction, **(c)** similar cuts of the ion and electron velocities in the out-of-plane direction. In the simulations, magnetic field strengths and particle number densities are normalized to arbitrary values B_0 and n_0 , respectively. Lengths are normalized to the ion inertial length $d_{i0} = c/\omega_{pi0}$ at the reference density n_0 . Time is normalized to the ion cyclotron time $(\Omega_{ci0})^{-1} = (eB_0/m_i c)^{-1}$. Speeds are normalized to the Alfvén speed $v_{A0} = B_0/(\mu_0 m_i n_0)^{1/2}$. Electric fields and temperatures are normalized to $E_0 = v_{A0} B_0/c$ and $T_0 = m_i v_{A0}^2$, respectively. The initial configuration in the system is such that the inflow reconnecting magnetic field is B_0 and the inflowing density is n_0 . Figure adapted from Shay et al. (1999)

does not necessarily imply that the spacecraft is in the ion diffusion region. To recognize a candidate diffusion region encounter one needs to rely on other predicted signatures such as the presence of strong field-aligned temperature anisotropy in the inflow region (e.g., Swisdak et al. 2005; Chen et al. 2008a; Egedal et al. 2010), or a strong out-of-the-plane current/an extremely thin (electron skin depth-scale) current sheet at the neutral sheet.

The challenges associated with the identification of the diffusion region when the crossing is normal to the current sheet can be alleviated by multi-spacecraft observations. If the inner electron diffusion region is as short (along the outflow direction) as predicted, there is a good chance that there will be spacecraft on opposite sides of the X-line and the presence of the X-line could be deduced by the detection of diverging electron jets.

Fig. 3 Particle-in-cell (PIC) simulation of asymmetric reconnection. **(a)** Outflow velocity, **(b)** out-of-plane magnetic field, **(c)** electric field normal to the current sheet, **(d)** normal component of the ion frozen-in condition, and **(e)** electron anisotropy. The *green line* in Panel **(e)** marks the first reconnected field line on the low-density side of the current sheet. The unit normalizations are the same as in Fig. 2. In the simulation, with the two inflow regions labeled “1” and “2”, the initial inflow conditions in code normalizations are $B_1 = 1.0$, $B_2 = 2.0$, $n_1 = 1.0$, $n_2 = 0.1$, $T_{e1} = 0.67$, $T_{e2} = 1.67$, $T_{i1} = 1.33$, $T_{i2} = 3.33$. Note that this run is nearly identical to run 1 from Table I of Malakit et al. (2013), except the simulation domain size is $102.4d_{i0}$ by $51.2d_{i0}$. Figure adapted from Malakit et al. (2013)



2.2 Magnetopause

In contrast to magnetotail reconnection which generally has almost symmetric inflow conditions and a small guide field, reconnection at the magnetopause usually involves highly asymmetric inflow density and magnetic field conditions (with the exception of a nearly symmetric event reported by Mozer et al. (2002)), and typically there is a substantial guide field. At the magnetopause spacecraft crossings of the diffusion region can occur either along the outflow direction (e.g., Phan et al. 2003; Retinò et al. 2005) or normal to the current sheet (e.g., Mozer et al. 2002). For spacecraft crossings of the diffusion region along the outflow direction (e.g., Phan et al. 2003; Retinò et al. 2005), some of the large-scale signatures, namely the reversals of outflow jets (Fig. 3(a)) and normal magnetic field, are similar to those described above for symmetric reconnection in the magnetotail.

It is more challenging to recognize a diffusion region crossing of asymmetric reconnection if the crossing is normal to the current sheet as many of the signatures that one normally would associate with the diffusion region also occur downstream of the

X-line. For example, since the Hall magnetic field pattern is bipolar in asymmetric reconnection rather than quadrupolar, an ion diffusion region crossing normal to the current sheet would detect a monopolar out-of-plane magnetic field (Fig. 3(b)) (e.g., Tanaka et al. 2008). However, a crossing of the reconnection exhaust far downstream of the diffusion region would also detect a monopolar out-of-plane magnetic field as part of the MHD rotational discontinuity that characterizes the reconnecting magnetopause (e.g., Levy et al. 1964; Sonnerup et al. 1981).

Furthermore, the violation of the ion frozen-in condition does not appear to be a clear indicator of the proximity to the X-line since this condition is violated all along the magnetospheric separatrix (Fig. 3(d)). Thus to distinguish between crossings of the diffusion region itself, versus crossings of the exhaust far downstream, one needs to identify plasma and field properties unique to the diffusion region or to its surroundings. For example, possible signatures of the electron diffusion region include theoretical predictions of enhanced dissipation (Zenitani et al. 2012) or non-gyrotropic electron distributions (e.g., Scudder et al. 2012; Aunai et al. 2013). Some of these features (e.g., non-gyrotropic electrons), however, also seem to extend far downstream of the diffusion region (e.g., Aunai et al. 2013). Furthermore, these parameters are difficult to measure accurately and will require substantial calibrations before they can be used.

A complementary approach is to examine the large-scale context of the region around the asymmetric reconnection diffusion region. For example, Malakit et al. (2013) predicted the presence of an earthward pointing “Larmor electric field” in the low-density (magnetospheric) inflow region that only appears within ~ 20 ion skin depths downstream of the X-line in their particle-in-cell simulations. The exact downstream extent of the Larmor electric field region could depend on the inflow parameters as well as the ion-to-electron mass ratio used in the simulation. While this electric field is not associated with electron physics in the diffusion region, it could provide the context for diffusion region crossings when the trajectory is normal to the magnetopause current sheet. Under typical ion temperature and magnetic field conditions in the magnetosheath ($T_i \sim 200$ eV, $B \sim 20$ nT) and magnetosphere ($T_i \sim 2$ keV, $B \sim 50$ nT), this field has been estimated to be ~ 20 mV/m, while the width (along the current normal) of the region is approximately twice the magnetospheric ion gyroradius, or ~ 120 km and should be measureable by MMS (Malakit et al. 2013).

Another feature that could be indicative of the proximity to the X-line is the enhancement of the electron temperature anisotropy in the magnetospheric inflow region (Fig. 3(e)), in the same region where the Larmor electric field appears. This is different from the temperature anisotropy enhancements seen downstream of the X-line which is located inside the exhaust near its magnetospheric edge.

Finally, near the X-line the current layers associated with the ion and electron diffusion regions are expected to be of ion and electron skin depth scales, respectively. The exhaust width expands with increasing distance from the X-line. Thus with the accurate determination of the current sheet width using closely spaced multi-point MMS measurements, it should be possible to deduce whether the spacecraft are close to the X-line or not.

2.3 Contrasting Reconnection X-Lines and O-Lines (Flux Rope) Signatures

In studies of reconnection, correlated reversals in the reconnection jets and normal magnetic field are widely considered to be the signature of the passage of a reconnection X-line, both at the dayside magnetopause and in the magnetotail. This signature has been used in many studies to identify diffusion region encounters, and also in developing statistics that are used to characterize the average location of reconnection sites in the magnetotail. However, multi-spacecraft studies in the magnetotail (e.g., Eastwood et al. 2005) and at the magnetopause

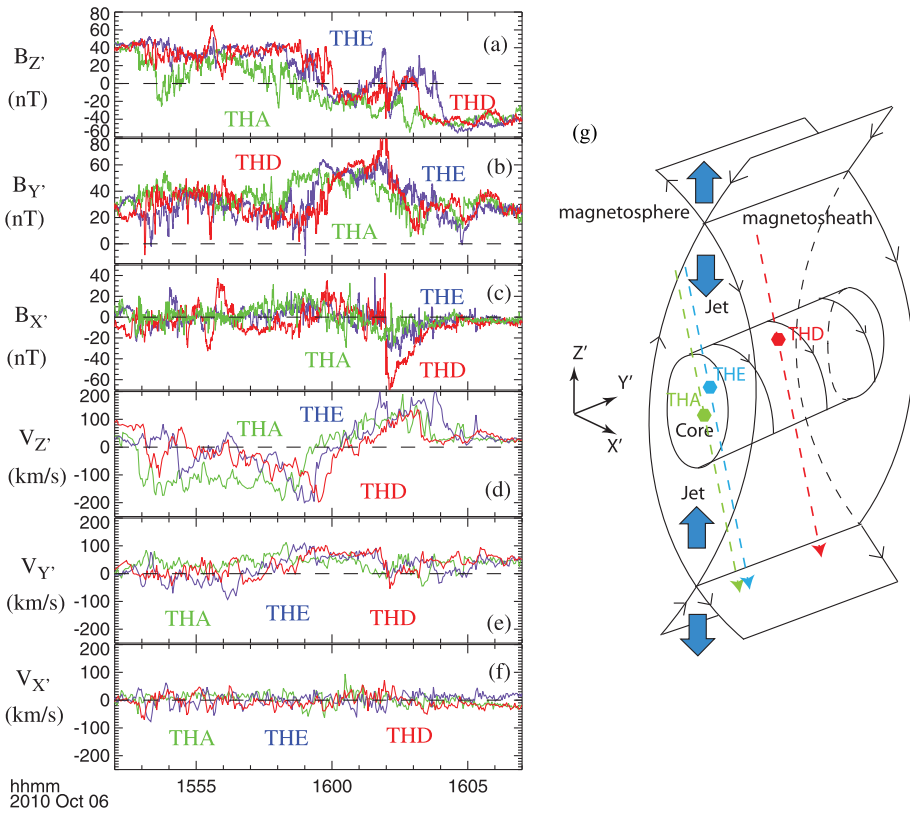


Fig. 4 Detection of a 3-D flux rope deduced from multi-point observations by three THEMIS spacecraft. (a) reconnecting magnetic field component, (b) out-of-plane magnetic field, (c) normal magnetic field, (d)–(f) ion velocity components along the outflow, out-of-plane, and normal directions, (g) a simplified sketch illustrating the large-scale features of the observed magnetic flux rope deduced from the three-spacecraft data. The reversal of the outflow jet (Panel d) in this event occurs at an O-line rather than an X-line. Figure adapted from Oieroset et al. (2011)

(e.g., Hasegawa et al. 2010; Oieroset et al. 2011) have shown that this signature alone can be misleading. Signatures that conventionally would be interpreted as a single X-line moving in one direction could in fact be an O-line (at the center of a flux rope bounded by two active X-lines) moving in the opposite direction. Multi-spacecraft observations, however, can help distinguish between X-line and O-line encounters.

Figure 4 shows an example observed by three THEMIS spacecraft at the magnetopause (Oieroset et al. 2011). The sketch (Panel g) depicts the observed flux rope with the spacecraft trajectories marked. On October 6, 2010 at ~15:00–16:00 UT the THEMIS A (THA), THEMIS E (THE), and THEMIS D (THD) spacecraft traversed the dayside subsolar magnetopause on an outbound pass. THA and THE were located at the same meridian at 12.6 Magnetic Local Time (MLT), with a Z_{GSM} separation of $0.174R_E$ (1107 km). THD was located slightly duskward at 12.8 (MLT), $0.0874R_E$ (557 km) northward of THE. The spacecraft data is presented in the magnetopause current sheet coordinate system, with x' along the current sheet normal (toward the Sun), y' along the X-line (toward dusk) and z' along the reconnection outflow direction (toward north). This coordinate system is close to the usual

GSM coordinate system. At $\sim 16:00$ UT all three spacecraft observed the reconnection outflow jet (V'_z) reversal (Panel d) during the current sheet crossing indicated by the B'_z gradient (Panel a).

The negative to positive V'_z reversal observed by the three spacecraft could be due to either an X-line moving south, in the $-z'$ direction, or a flux rope, flanked by 2 active X-lines, moving north, in the $+z'$ direction. With spacecraft separated in the z' direction, one could conclusively distinguish between these two scenarios. In the former (X-line) scenario, the northern-most spacecraft (THD) would detect the flow reversal first, followed by THE and THA. In the latter (flux rope) scenario, THD would observe the flow reversal last. Panel d shows that the flow reversal was first detected by THA, followed by THE and then THD, which implies a northward moving structure. Furthermore, the out-of-plane magnetic field B'_y (Panel b) was strongly enhanced, especially at THD and THE, in the vicinity of the flow reversal region, which is typical of flux ropes. In other words, the northward moving structure was a flux rope (O-line) with a strong core field instead of a southward moving X-line.

With the availability of multi-point MMS measurements, using similar analyses as the one described above one will be able to reliably distinguish between X-line and O-line encounters.

3 Strategies for Capturing and Transmitting Burst Data in the Diffusion Region

The success of the MMS mission in solving the microphysics of reconnection depends critically on the ability of the mission to return the highest resolution data in the reconnection diffusion region. Because of the minuscule size of the diffusion region, the total number of diffusion regions encountered by the MMS spacecraft will be small during its mission; it is estimated that there will be 63 magnetopause ion diffusion region encounters during the two dayside seasons (Griffiths et al. 2011; Fuselier et al. 2015, [this issue](#)), and ~ 7 ion diffusion region encounters in the magnetotail during the single nominal mission tail season (Genestreti et al. 2013). Since many events (for various boundary conditions) are required to provide science closure, the MMS burst triggers need to be able to capture close to all of the diffusion regions encountered by the spacecraft. Such a requirement on a mission is unprecedented, considering the fact that only a small fraction (~ 20 minutes per day or $\sim 2\%$) of the high-resolution data collected over an orbit can be transmitted to ground. This poses significant challenges for the MMS mission because the transmitted burst data needs to contain the occasional diffusion region encounters. Consequently, the burst data capture scheme must be extremely robust.

MMS will implement an automated burst trigger scheme to identify candidate diffusion regions, complemented by a scheme which involves a Scientist-In-The-Loop (SITL) who will serve to verify and improve the burst data selections. Once the diffusion region candidates are identified, the next challenge is to transmit all of them to ground. To accomplish the latter, MMS will have a 96 Gigabyte onboard memory that allows the collection of burst data continuously through several orbits. Summary data, such as lower-resolution plasma moments and fields, are transmitted to ground each orbit, and are used by the SITL to hand pick diffusion region candidates to be transmitted at the high data rate during subsequent orbit(s). Automated burst trigger algorithms play a significant role in such a system since they provide candidate events that the SITL can verify, optimize, and approve. Such a combined scheme would ensure that 100% of the transmitted burst data are of prime science interest,

and that decisions can be made by the SITL in as efficient manner as possible in what may be a time-constrained situation. In the following sections, we will describe how the burst system could work for the magnetopause and magnetotail.

3.1 Magnetopause

Capturing All Magnetopause Crossings One could attempt to capture diffusion region crossings based on the expected large-scale contexts (e.g., flow and normal field reversals, or the presence of the Larmor electric field in the inflow region) described in Sect. 2. However, there is a simpler approach for the magnetopause: since reconnection occurs in magnetopause current sheets, if burst data from all magnetopause crossings can be transmitted, no diffusion regions encountered by the spacecraft would be missed. The advantage of this approach is that one does not rely on predicted kinetic or even large-scale signatures of the diffusion region, thus one is not biased toward a certain theory/model. Furthermore, magnetopause crossings are easily captured by automated algorithms or by the SITL based on low-resolution survey data. The feasibility of the approach of transmitting all magnetopause burst data, however, depends on the volume of magnetopause data, which in turn depends on the number of MMS magnetopause crossings and their durations. We now estimate these numbers based on data from the THEMIS mission.

Expected MMS Burst Data Volume and Data Storing Schemes To better understand MMS' likely observations, we examine the THEMIS 2009 dayside season. In particular, we focus on two of the THEMIS probes: at this time THEMIS-D had a $12R_E$ apogee orbit with sidereal period, hence identical to the orbit proposed for MMS dayside phase, and THEMIS-A had a apogee of $13R_E$ which is being considered for the later part of the MMS second dayside season. Figure 5 shows an example of 10 complete magnetopause crossings during a single THEMIS-D dayside orbit. The magnetopause crossings are characterized by density gradients (Panel b) and magnetic field rotations (Panel d). Figure 5 illustrates a key issue which is that because of boundary motion, there can be numerous magnetopause crossings on any particular orbit.

Figures 6 and 7 show the distribution of magnetopause crossings by THEMIS-D and THEMIS-A, respectively, over a period of 6 months as the spacecraft orbits precessed from Dusk to Dawn, through the subsolar region. Panel a of each figure shows that the number of crossings per day varied significantly from one day to the next; some days had more than 30 crossings while others had none. The total number of magnetopause crossings by THEMIS-D was 917, versus 1379 crossings for THEMIS-A. Thus the higher apogee spacecraft had more magnetopause crossings. This is expected because while the nominal magnetopause distance at the subsolar point is $\sim 10\text{--}12R_E$, it expands towards $15R_E$ near the terminators. Therefore with its apogee of $13R_E$ THEMIS-A has additional opportunities of magnetopause encounters further away from noon as compared to THEMIS-D. Panel c of each figure shows the number of crossings as a function of local time. As expected, the spacecraft with $13R_E$ apogee (THEMIS E) had more flank (away from 12 MLT) magnetopause crossings than the spacecraft with $12R_E$ apogee (THEMIS-D). Also, as expected, the lower apogee spacecraft had more subsolar magnetopause crossings.

In terms of magnetopause data volume, what is more important to know is the total duration of magnetopause crossings per day. In our survey, the time interval (duration) of each complete magnetopause encompasses the full magnetic field rotation and density gradient across the magnetopause, in addition to short intervals of the adjacent magnetosheath and magnetosphere. The durations of magnetopause crossings vary from case to case and are

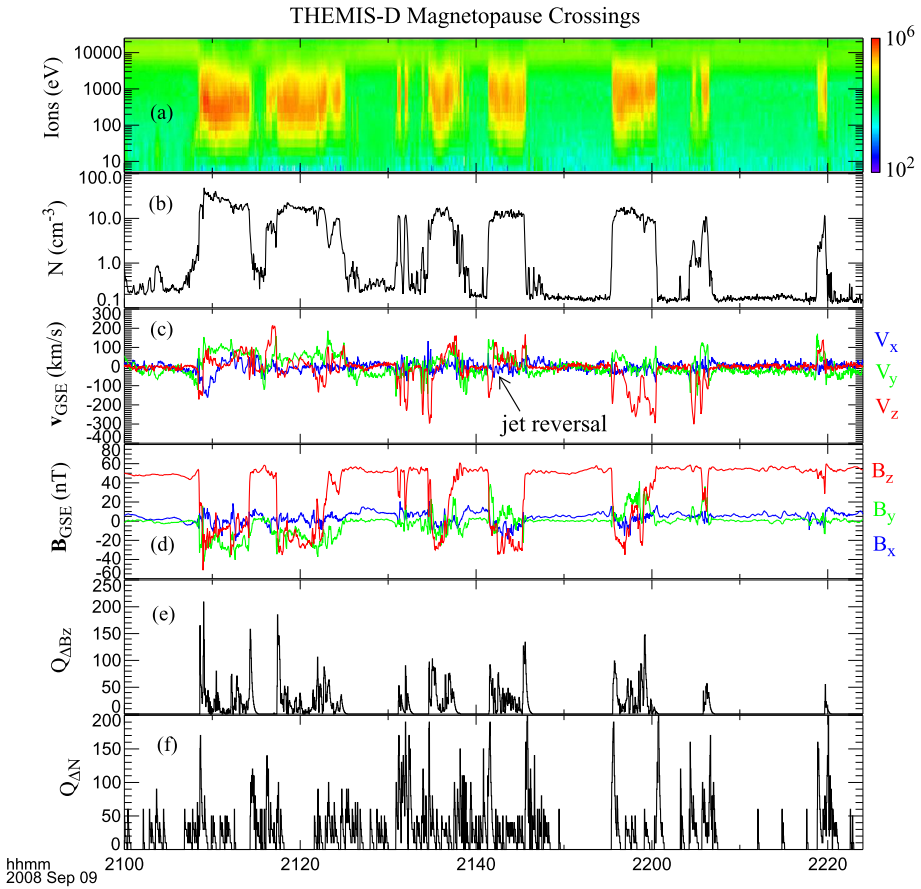


Fig. 5 Example of multiple crossings of the magnetopause in the subsolar region and the performance of automated burst triggers. **(a)** Ion spectrogram, **(b)** ion density, **(b)** ion velocity in GSE coordinate system, **(d)** magnetic field in GSE, **(e)** quality value $Q_{\Delta B_z}$ based on gradients in 3-s resolution B_z , and **(f)** quality value $Q_{\Delta N}$ based on gradients in 3-s resolution plasma density. Both $Q_{\Delta B_z}$ and $Q_{\Delta N}$ are enhanced at magnetopause crossings

dependent on the thickness of the magnetopause and its motion relative to the spacecraft. The average duration of a magnetopause crossing in our dataset is ~ 2 minutes. Panel b of Figs. 6 and 7 shows the total duration of magnetopause crossings per day. Some days had durations of more than 70 minutes, greatly exceeding the daily average amount (~ 20 minutes) of burst data than can be transmitted, while other days were well below the 20-min limit. To be able to transmit all the magnetopause burst data, each MMS spacecraft will in fact be able to store in its entirety 2–4 days worth of all the highest resolution data. Consequently, if there are too many magnetopause encounters on a particular day, these data can be stored and transmitted on subsequent days. However, because there are consecutive days when the total amount of magnetopause data far exceeds 20 minutes, storing 2–4 days of full orbit data still would not allow the transmission of all magnetopause crossings. Thus, the planned strategy (Fuselier et al. 2015, [this issue](#)) is to allocate a portion of the 96GB memory to storing shorter data intervals containing magnetopause intervals over a period of several weeks to ensure that all magnetopause data can be transmitted during a later stage

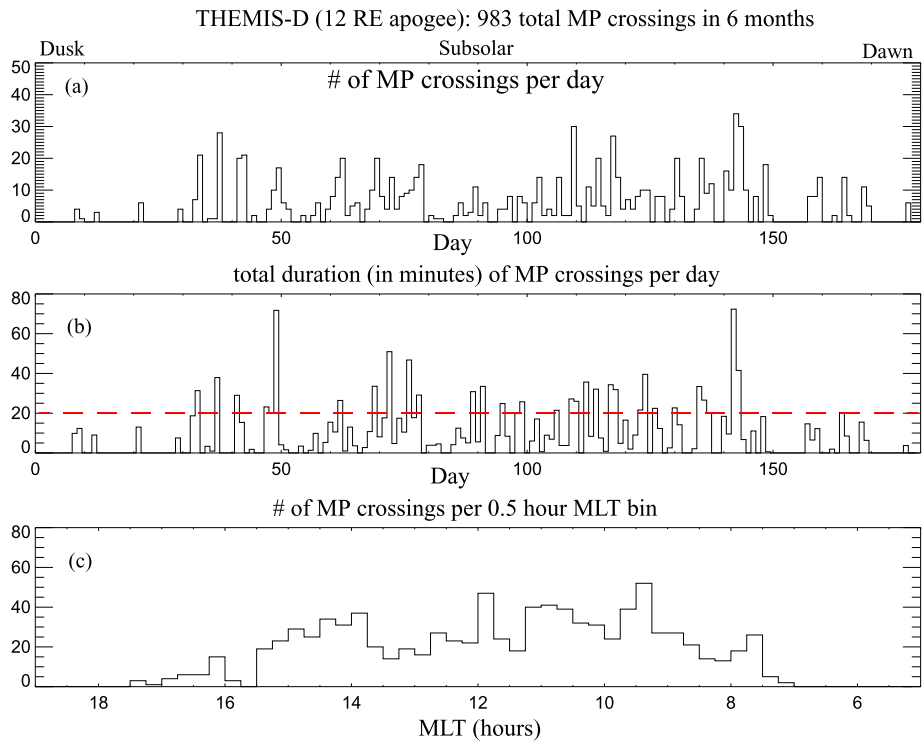


Fig. 6 Statistical survey of all complete magnetopause crossings by THEMIS-D which had a $12-R_E$ apogee in 2009. **(a)** Number of magnetopause crossings per day for a 6-month dayside phase, **(b)** total duration of magnetopause crossings per day, and **(c)** number of magnetopause crossings as a function of the magnetic local time (MLT). The red dashed line in Panel **(b)** marks the daily average amount (20 minutes) of burst data that can be transmitted to ground

of the dayside season when the orbits approach the dawn terminator where magnetopause crossings are less frequent.

The total duration of all magnetopause intervals for THEMIS D over a 6-months dayside season in 2008 was 1640 minutes, and 2775 minutes for THEMIS A. These numbers compare favorably to the nominal 3600 minutes of burst data that can be transmitted during the 6-month period, indicating that in principle, burst data of all complete magnetopause crossings can be transmitted to ground using the scheme described above.

3.2 Magnetotail

Reconnection-Associated Phenomena in the Magnetotail In addition to diffusion region physics, of interest are kinetic physics in reconnection exhausts (bursty bulk flows), exhaust boundaries and separatrices, and reconnection jet fronts (also called “dipolarization fronts”) (e.g., Nakamura et al. 2002; Runov et al. 2009) which may be important sites for particle energization (Angelopoulos et al. 2013). The planned MMS orbit is such that during the first science tail season (phase 1x), the apogee will be $12R_E$, with the apogee being raised to $25R_E$ for the second science tail season (phase 2b) (Fuselier et al. 2015, this issue). Consequently, reconnection jet fronts will be the primary target of MMS during the first sci-

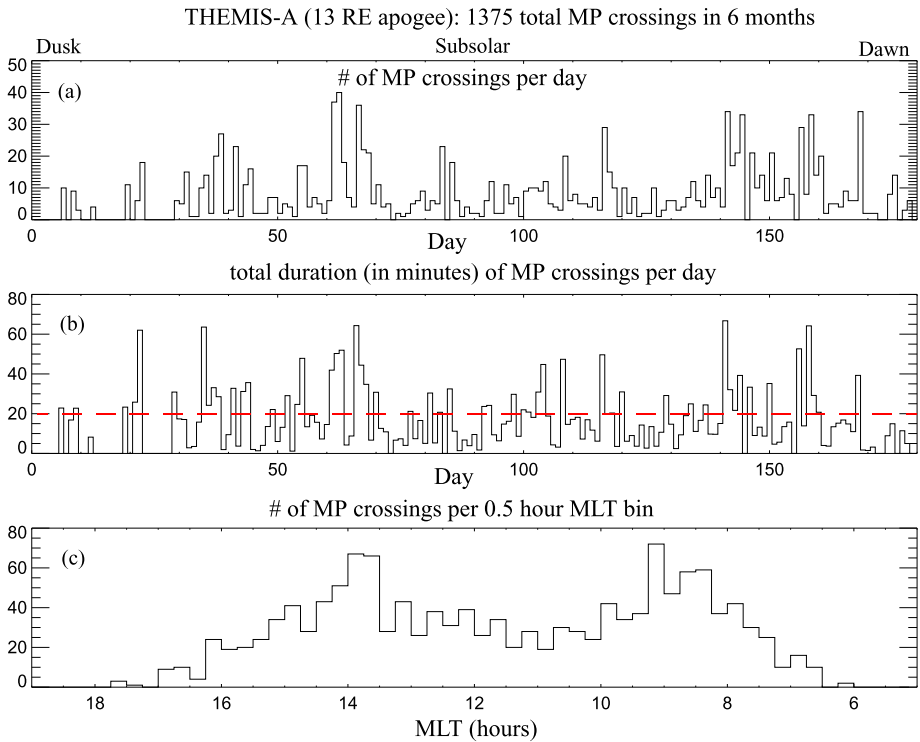


Fig. 7 Statistical survey of all complete magnetopause crossings by THEMIS-A which had a $13-R_E$ apogee in 2009. The format is the same as in Fig. 6. Because of its higher apogee, THEMIS-A had $\sim 30\%$ more magnetopause crossings than THEMIS-D, with more crossings occurring 2 hours (in MLT) away from the subsolar point

ence tail season, with the diffusion region itself of more importance in the second science tail season.

It would be ideal if one could transmit burst data for all these phenomena similar to the magnetopause case. However, as we shall describe below, the volume of burst data associated with all these reconnection phenomena together is expected to exceed the total telemetry capacity (3600 minutes of burst data per 6 months tail season). Thus it will be necessary to prioritize which events are of primary interest. Based on our survey of THEMIS magnetotail data, the data volumes corresponding to diffusion region candidates, jet fronts, and exhaust boundaries are relatively small so that all such data can be transmitted. On the other hand, less than 50% of all reconnection exhaust (bursty bulk flow) burst data can be transmitted. But since exhaust encounters are abundant, capturing a representative fraction of such events should be sufficient.

Diffusion Region Candidates Because reconnection in the near-Earth magnetotail is highly bursty and short-lived (typically lasting ~ 10 – 20 minutes) (e.g., Baumjohann et al. 1990; Angelopoulos et al. 1992, 1994), the chance of a spacecraft crossing the diffusion region is low. A survey of THEMIS-B data from the 2009 tail season, when its orbit apogee was $\sim 30R_E$, found a total of 14 obvious ion diffusion region candidates over a tail season. These candidates were identified by tailward to earthward flow reversal and concurrent negative to positive B_z reversals (see example in Figs. 8(j), (k)) that are most likely associated the

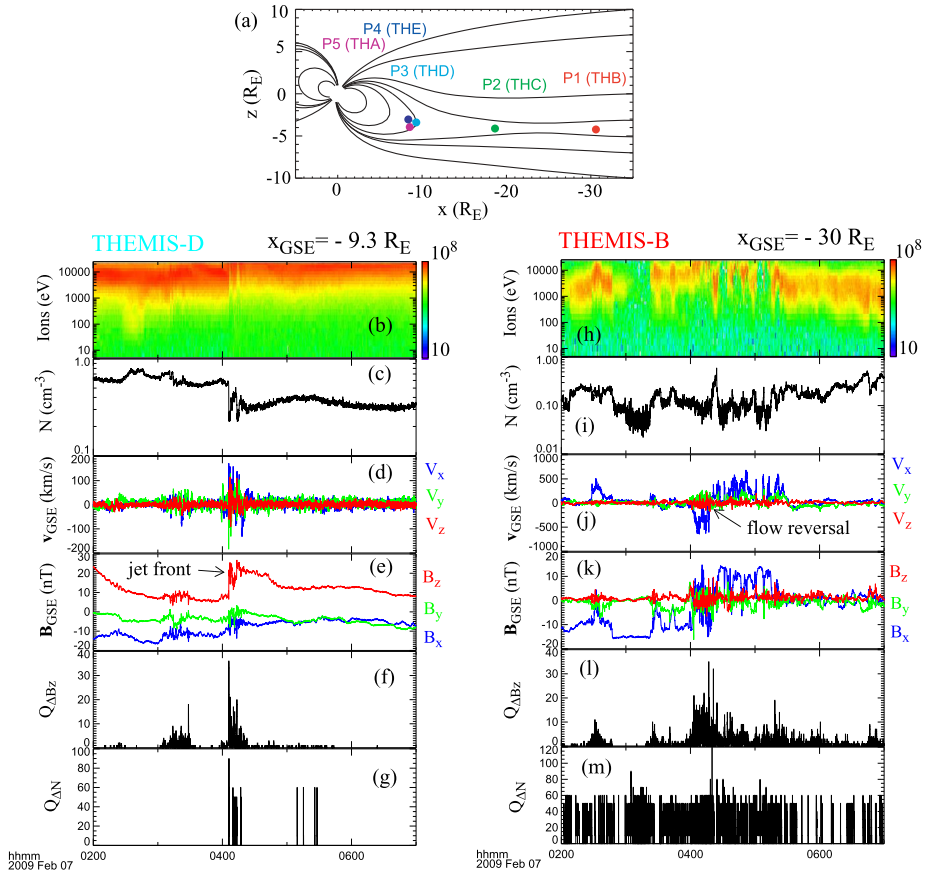


Fig. 8 Examples of the detection of reconnection jet front and a candidate diffusion region and the performance of the automated burst triggers. (a) schematic showing the positions of the five THEMIS spacecraft on February 7, 2009, (b) and (h) Ion spectrogram, (c) and (i) ion density, (d) and (j) ion velocity in GSE, (e) and (k) magnetic field in GSE, (f) and (l) quality value $Q_{\Delta B_z}$ based on gradients in 3-s resolution B_z , (g) and (m) quality value $Q_{\Delta N}$ based on gradients in 3-s resolution plasma density. $Q_{\Delta B_z}$ is enhanced at the jet front as well as the in the vicinity of the candidate X-line

tailward retreat of the X-line (see also Eastwood et al. 2010b). While these signatures could be due to earthward moving flux rope as discussed in Sect. 2.3, such a scenario is probably less likely because the dominant reconnection X-lines and O-lines in the near-Earth magnetotail should be moving tailward because of the higher downstream pressure on the earthward side of the X-line (e.g., Oka et al. 2011). The THEMIS-B data in our survey was taken in 2009 during solar minimum. It is possible that MMS will encounter more diffusion regions during solar maximum (Nagai et al. 2005). But even if we double the number of estimated magnetotail diffusion region candidates to 30, with each event lasting on average 30 minutes (which includes not only the diffusion region but also the exhausts on both sides of the X-line) all the burst data of can be transmitted to ground during a 6-month tail season, with 75 % of the telemetry still available for capturing other phenomena.

Our survey does not include events in which the spacecraft crosses the diffusion region along the current sheet normal but staying on one side of the X-line during the crossing.

Such events would not show correlated plasma jet and normal magnetic field reversals. In the magnetotail, such events are likely to be less common than flow reversal events because of the tendency for the X-line to retreat tailward such that flow reversals most likely occur when spacecraft encounters the diffusion region.

Reconnection Jet Fronts In contrast to the rarity of diffusion region crossings, there are usually multiple spacecraft encounters with the reconnection exhaust jets and the jet fronts every orbit. The jet front is characterized by a sudden and sharp increase of the normal magnetic field component B_z lasting typically <30 s, followed by the full jet (see Fig. 8(d) and (e) for an example). Our survey of data from THEMIS-D, which had an apogee of $12R_E$ similar to MMS apogee during mission phase 1x, found ~ 110 jet fronts in the 2009 magnetotail season. Since MMS will be at higher distances from the neutral sheet in phase 1x, it will be observing the field aligned flows and active boundary layer beams related to the approaching reconnection jets (Zhou et al. 2012), rather than the jet fronts at the neutral sheet. These field aligned flows and beams are expected to have similar occurrence rates as the reconnection jets themselves. Lower occurrence rates (by a factor of 4) of reconnection jets are observed near the phase 2b MMS apogee in the tail, at $\sim 25R_E$ (Liu et al. 2013; Fig. 2(c)). If one were to collect burst data only at the front of the jet where the sharpest gradients occur, the total duration of burst data for the 2009 THEMIS tail season would be ~ 55 minutes, well within the telemetry capacity over a full tail season.

Exhaust Boundaries/Separatrices The exhaust boundaries are of interest because of the possible presence of slow shocks there that could energize particles (e.g., Feldman et al. 1985; Saito et al. 1998), and kinetic Alfvén wave physics that is associated with enhanced Poynting flux and super-Alfvénic signal propagation (Shay et al. 2011). Because these boundaries are sharp (thus their crossing durations are short), their associated burst data can all be transmitted to ground.

Full Reconnection Jets (Also Called Bursty Bulk Flows) Behind the jet front is the full plasma jet that typically lasts 10–20 minutes. If 400 jets are detected as was the case for the THEMIS-B 2009 tail season, the amount of full jet data (up to 8000 minutes) would exceed the telemetry capability by more than a factor of two. Thus prioritization of such events will be needed. A possible consideration is to emphasize events with the largest energy conversions as indicated by high levels of energetic particle fluxes or high flow speeds. Another possible emphasis is on events that display multiple rapid magnetic dipolarizations that are embedded within bursty bulk flows. Such events have been found to dominate flux transport in the magnetotail (Liu et al. 2014) and correlate with particle acceleration and heating (Gabrielse et al. 2014), as well as intense energy conversion (Angelopoulos et al. 2013).

3.3 Automated Burst Trigger Schemes

One of the key components of the burst data management scheme is the implementation of automated burst trigger algorithms designed to capture the magnetopause current sheet on the dayside and reconnection-related phenomena on the night side. The automatic selection of burst intervals will be validated or adjusted using low-resolution survey data by the Scientist-In-The-Loop (SITL). In this section we describe some examples of the schemes that are being tested for MMS and their performance based on test (THEMIS) data. Some of these schemes have been used by the THEMIS and Wind missions to capture essentially the same reconnection phenomena and they could be further optimized for MMS.

The magnetopause is characterized by a spatial gradient in the density and rotation of the magnetic field, while bursty reconnection in the tail leads to sudden changes in the flow and fields as well as enhancements of the plasma wave activities. Spatial gradients and temporal variations both manifest themselves as rapid variations of plasma and field parameters observed by a spacecraft. A simple gradient-based trigger algorithm used by the Wind and THEMIS missions is now described. The rating of the “Quality” (Q) factor of these large variations is based on the following formula: $Q = |\text{data} - \text{smoothed_data}|$ where $\text{smoothed_data}_{j+1} = (\text{smoothed_data}_j(2^M - 1) + \text{data}_j)/2^M$, and M is an adjustable parameter that controls the degree of data smoothing. On Wind and THEMIS, M is set to 2 when the formula is applied to 3-s resolution data. This algorithm has been successfully used to capture the magnetopause on the dayside (e.g., Phan et al. 2001, 2013) and bursty bulk flows (e.g., Raj et al. 2002), diffusion region candidates (Angelopoulos et al. 2008; Oka et al. 2011) and reconnection jet fronts (e.g., Runov et al. 2009) in the magnetotail. We now describe the operation of the trigger algorithm at the magnetopause and in the tail with some THEMIS examples.

Dayside Magnetopause Figure 5 shows an example of the operation of triggers based on the density and magnetic field B_z gradients at the multiple crossings of the magnetopause. The magnetopause crossings are recognized by magnetic field rotation from $B_z < 0$ in the magnetosheath to $B_z > 0$ in the magnetosphere (Panel d) and density gradients (Panel b). Panels e and f display the Quality values $Q_{\Delta B_z}$ and $Q_{\Delta N}$ computed using the formula above on the magnetic field component B_z (in GSM coordinates) and on plasma density using 3-s resolution data, respectively. It is seen that both $Q_{\Delta B_z}$ and $Q_{\Delta N}$ are enhanced at all magnetopause crossings, including a diffusion region candidate at $\sim 21:41$ UT. The locations of the peak $Q_{\Delta B_z}$ and $Q_{\Delta N}$ differ slightly; with $Q_{\Delta B_z}$ peaking at the outer (magnetosheath) side of the magnetopause where the field rotation is largest, whereas $Q_{\Delta N}$ tends to peak at the magnetospheric edge of the magnetopause where the density gradient is largest. These examples suggest that the magnetopause can be captured using a combination of density and B_z triggers to ensure that the entire magnetopause interval is captured. Furthermore, the MMS scientist in the loop (SITL) will be able to examine the survey data, together with the computed trigger quality values to optimize the burst data intervals.

We have also found that plasma wave activity is usually enhanced in the magnetopause (compared to the magnetosphere). However, because the wave power is also typically enhanced in the magnetosheath, a burst trigger based on the intensity of wave activities does not work as well.

Magnetotail Although the physics at the X-line, in the exhaust or at its boundaries in bursty magnetotail reconnection might be different, a common signature detected by a spacecraft of these phenomena is the sudden enhancement of the magnetic field fluctuations (indicative of active current sheets) compared to the magnetic field condition in the quiet magnetotail current sheet before the onset of reconnection. Testing the various trigger algorithms on THEMIS we found that the gradient-based burst trigger using 3-s resolution magnetic field $B_{GSM,z}$ works quite well to capture most reconnection-related phenomena, although other parameters such as wave power could also be used.

Figure 8(h)–(m) show 5 hours of THEMIS-B observations around a diffusion region candidate when the spacecraft was at its apogee, $\sim 30R_E$ behind the Earth. The possible crossing of tailward retreating X-line is evidenced by the tailward to earthward V_x flow reversal and predominantly negative to positive B_z reversal. Figure 8(l) show that $Q_{\Delta B_z}$ was enhanced throughout the plasma jetting interval ($\sim 04:00$ – $05:15$ UT), with the largest

enhancement being close to the flow reversal (at $\sim 04:10$ UT). This also means that an extended interval where $Q_{\Delta B_z}$ is enhanced could be used as a guide to identify the duration of the burst mode interval that must be transmitted to the ground.

On THEMIS we have also found that the same B_z trigger can reliably capture reconnection jet fronts and the full jet as well. Figure 8(b)–(g) shows an example of a reconnection jet and its front at $\sim 04:05$ UT. $Q_{\Delta B_z}$ was strongly enhanced at the jet front as well as in the plasma jet behind it.

Finally, it is noted that a trigger based on gradients in B_x would work equally well (not shown), thus either B_x or B_z , or a combination of the two, could be used as a trigger parameter in the magnetotail to capture active current sheets.

4 Summary and Conclusions

The success of the MMS mission in understanding the microphysics of magnetic reconnection depends on its ability to return the highest resolution measurements of the minuscule reconnection diffusion region. The present paper describes the efforts by our Inter-Disciplinary Scientist (IDS) team to (a) establish the large-scale contexts for reconnection diffusion region encounters that would help the identification of diffusion regions in spacecraft data, and (b) devise possible strategies for capturing and transmitting burst data of all diffusion region candidates, in addition to data in the reconnection exhaust and its boundaries. Based on our experience with THEMIS observations, it is estimated that burst data from all MMS magnetopause crossings can be transmitted to ground such that no magnetopause reconnection diffusion regions or exhausts encountered by the spacecraft will be missed. In the magnetotail where the data volume of all reconnection related phenomena exceed telemetry capabilities, our survey of THEMIS data suggests that MMS will still be able to transmit burst data of all encounters with the diffusion regions, reconnection jet fronts, and separatrixes, but less than 50 % of the encounters with full reconnection jets.

With the knowledge of the properties of the region surrounding the diffusion region and the combination of automated burst triggers and further optimization by the Scientist-In-The-Loop, MMS should be able to capture most diffusion regions it encounters and achieve its prime science objectives.

Acknowledgements We thank John Bonnell, Peter Harvey, and Davin Larson for their role in the development of the THEMIS and Wind burst trigger schemes. This research was funded by NASA grants NNX08AO83G and NNX11AD69G. Simulations and analysis were performed at the National Center for Atmospheric Research Computational and Information System Laboratory (NCAR-CISL) and at the National Energy Research Scientific Computing Center (NERSC). We wish to acknowledge support from the International Space Science Institute in Bern, Switzerland.

Open Access This article is distributed under the terms of the Creative Commons Attribution 4.0 International License (<http://creativecommons.org/licenses/by/4.0/>), which permits unrestricted use, distribution, and reproduction in any medium, provided you give appropriate credit to the original author(s) and the source, provide a link to the Creative Commons license, and indicate if changes were made.

References

- V. Angelopoulos, W. Baumjohann, C.F. Kennel, F.V. Coronti, M.G. Kivelson, R. Pellat, R.J. Walker, H. Luehr, G. Paschmann, Bursty bulk flows in the inner central plasma sheet. *J. Geophys. Res.* **97**, 4027–4039 (1992). doi:[10.1029/91JA02701](https://doi.org/10.1029/91JA02701)

- V. Angelopoulos, C.F. Kennel, F.V. Coroniti, R. Pellat, M.G. Kivelson, R.J. Walker, C.T. Russell, W. Baumjohann, W.C. Feldman, J.T. Gosling, Statistical characteristics of bursty bulk flow events. *J. Geophys. Res.* **99**, 21257 (1994). doi:[10.1029/94JA01263](https://doi.org/10.1029/94JA01263)
- V. Angelopoulos, J.P. McFadden, D. Larson, C.W. Carlson, S.B. Mende, H. Frey, T. Phan, D.G. Sibeck, K.-H. Glassmeier, U. Auster, E. Donovan, I.R. Mann, I.J. Rae, C.T. Russell, A. Runov, X.-Z. Zhou, L. Kepko, Tail reconnection triggering substorm onset. *Science* **321**, 931 (2008). doi:[10.1126/science.1160495](https://doi.org/10.1126/science.1160495)
- V. Angelopoulos, A. Runov, X.-Z. Zhou, D.L. Turner, S.A. Kiehas, S.-S. Li, I. Shinohara, Electromagnetic energy conversion at reconnection fronts. *Science* **341**, 1478–1482 (2013). doi:[10.1126/science.1236992](https://doi.org/10.1126/science.1236992)
- N. Aunai, M. Hesse, M. Kuznetsova, Electron nongyrotropy in the context of collisionless magnetic reconnection. *Phys. Plasmas* **20**, 092903 (2013). doi:[10.1063/1.4820953](https://doi.org/10.1063/1.4820953)
- W. Baumjohann, G. Paschmann, H. Luehr, Characteristics of high-speed ion flows in the plasma sheet. *J. Geophys. Res.* **95**, 3801–3809 (1990). doi:[10.1029/JA095iA04p03801](https://doi.org/10.1029/JA095iA04p03801)
- A.L. Borg, M. Oieroset, T.D. Phan, F.S. Mozer, A. Pedersen, C. Mouikis, J.P. McFadden, C. Twitty, A. Balogh, H. Réme, Cluster encounter of a magnetic reconnection diffusion region in the near-Earth magnetotail on September 19, 2003. *Geophys. Res. Lett.* **32**, 19105 (2005). doi:[10.1029/2005GL023794](https://doi.org/10.1029/2005GL023794)
- J.L. Burch, T.E. Moore, R.B. Torbert, B.L. Giles, MMS overview and science objectives. *Space Sci. Rev.* (2015, this issue)
- L.J. Chen, N. Bessho, B. Lefebvre, H. Vaith, A. Fazakerley, A. Bhattacharjee, P.A. Puhl-Quinn, A. Runov, Y. Khotyaintsev, A. Vaivads, E. Georgescu, R. Torbert, Evidence of an extended electron current sheet and its neighboring magnetic island during magnetotail reconnection. *J. Geophys. Res.* **113**, 12213 (2008a). doi:[10.1029/2008JA013385](https://doi.org/10.1029/2008JA013385)
- J.P. Eastwood, D.G. Sibeck, J.A. Slavin, M.L. Goldstein, B. Lavraud, M. Sitnov, S. Imber, A. Balogh, E.A. Lucek, I. Dandouras, Observations of multiple X-line structure in the Earth's magnetotail current sheet: a cluster case study. *Geophys. Res. Lett.* **32**, 11105 (2005). doi:[10.1029/2005GL022509](https://doi.org/10.1029/2005GL022509)
- J.P. Eastwood, T.-D. Phan, F.S. Mozer, M.A. Shay, M. Fujimoto, A. Retino, M. Hesse, A. Balogh, E.A. Lucek, I. Dandouras, Multi-point observations of the Hall electromagnetic field and secondary island formation during magnetic reconnection. *J. Geophys. Res.* **112**, A06235 (2007). doi:[10.1029/2006JA012158](https://doi.org/10.1029/2006JA012158)
- J.P. Eastwood, M.A. Shay, T.D. Phan, M. Oieroset, Asymmetry of the ion diffusion region hall electric and magnetic fields during guide field reconnection: observations and comparison with simulations. *Phys. Rev. Lett.* **104**(20), 205001 (2010a). doi:[10.1103/PhysRevLett.104.205001](https://doi.org/10.1103/PhysRevLett.104.205001)
- J.P. Eastwood, T.D. Phan, M. Oieroset, M.A. Shay, Average properties of the magnetic reconnection ion diffusion region in the Earth's magnetotail: the 2001–2005 cluster observations and comparison with simulations. *J. Geophys. Res.* **115**, 8215 (2010b). doi:[10.1029/2009JA014962](https://doi.org/10.1029/2009JA014962)
- J. Egedal, A. Lê, Y. Zhu, W. Daughton, M. Oieroset, T. Phan, R.P. Lin, J.P. Eastwood, Cause of super-thermal electron heating during magnetotail reconnection. *Geophys. Res. Lett.* **37**, L10102 (2010). doi:[10.1029/2010GL043487](https://doi.org/10.1029/2010GL043487)
- W.C. Feldman, D.N. Baker, S.J. Bame, J. Birn, J.T. Gosling, E.W. Hones Jr., S.J. Schwartz, Slow-mode shocks—a semipermanent feature of the distant geomagnetic tail. *J. Geophys. Res.* **90**, 233–240 (1985). doi:[10.1029/JA090iA01p00233](https://doi.org/10.1029/JA090iA01p00233)
- S.A. Fuselier, W.S. Lewis, C. Schiff, R. Ergun, J.L. Burch, S.M. Petrincic, K.J. Trattner, Magnetospheric multiscale science mission profile and operations. *Space Sci. Rev.* (2015, this issue). doi:[10.1007/s11214-014-0087-x](https://doi.org/10.1007/s11214-014-0087-x)
- C. Gabrielse, V. Angelopoulos, A. Runov, D.L. Turner, Statistical characteristics of particle injections throughout the equatorial magnetotail. *J. Geophys. Res. Space Phys.* **119**, 2512–2535 (2014). doi:[10.1002/2013JA019638](https://doi.org/10.1002/2013JA019638)
- K. Genestreti, S.A. Fuselier, J. Goldstein, T. Nagai, An empirical model for the location and occurrence rate of near-Earth magnetotail reconnection. *J. Geophys. Res.* **118**, 6389–6396 (2013). doi:[10.1002/2013JA019125](https://doi.org/10.1002/2013JA019125)
- S.T. Griffiths, S.M. Petrincic, K.J. Trattner, S.A. Fuselier, J.L. Burch, T.D. Phan, V. Angelopoulos, A probability assessment of encountering dayside magnetopause diffusion regions. *J. Geophys. Res.* **116**, A02214 (2011). doi:[10.1029/2010JA015316](https://doi.org/10.1029/2010JA015316)
- H. Hasegawa, J. Wang, M.W. Dunlop, Z.Y. Pu, Q.-H. Zhang, B. Lavraud, M.G.G.T. Taylor, O.D. Constantinescu, J. Berchem, V. Angelopoulos, J.P. McFadden, H.U. Frey, E.V. Panov, M. Volwerk, Y.V. Bogdanova, Evidence for a flux transfer event generated by multiple X-line reconnection at the magnetopause. *Geophys. Res. Lett.* **37**, 16101 (2010). doi:[10.1029/2010GL044219](https://doi.org/10.1029/2010GL044219)
- M. Hesse, K. Schindler, J. Birn, M. Kuznetsova, The diffusion region in collisionless magnetic reconnection. *Phys. Plasmas* **6**, 1781–1795 (1999). doi:[10.1063/1.873436](https://doi.org/10.1063/1.873436)
- R. Levy, H. Petscheck, G. Siscoe, Aerodynamic aspects of the magnetospheric flow. *AIAA J.* **2**, 2065 (1964)
- J. Liu, V. Angelopoulos, A. Runov, X.-Z. Zhou, On the current sheets surrounding dipolarizing flux bundles in the magnetotail: the case for wedgelets. *J. Geophys. Res.* **118**, 2000–2020 (2013). doi:[10.1002/jgra.50092](https://doi.org/10.1002/jgra.50092)

- J. Liu, V. Angelopoulos, X.-Z. Zhou, A. Runov, Magnetic flux transport by dipolarizing flux bundles. *J. Geophys. Res. Space Phys.* **119**, 909–926 (2014). doi:[10.1002/2013JA019395](https://doi.org/10.1002/2013JA019395)
- K. Malakit, M.A. Shay, P.A. Cassak, D. Ruffolo, New electric field in asymmetric magnetic reconnection. *Phys. Rev. Lett.* **111**, 033601 (2013). doi:[10.1103/PhysRevLett.111.135001](https://doi.org/10.1103/PhysRevLett.111.135001)
- F.S. Mozer, S.D. Bale, T.D. Phan, Evidence of diffusion regions at a subsolar magnetopause crossing. *Phys. Rev. Lett.* **89**(1), 015002 (2002). doi:[10.1103/PhysRevLett.89.015002](https://doi.org/10.1103/PhysRevLett.89.015002)
- T. Nagai, M. Fujimoto, R. Nakamura, W. Baumjohann, A. Ieda, I. Shinohara, S. Machida, Y. Saito, T. Mukai, Solar wind control of the radial distance of the magnetic reconnection site in the magnetotail. *J. Geophys. Res.* **110**, A09208 (2005). doi:[10.1029/2005JA011207](https://doi.org/10.1029/2005JA011207)
- T. Nagai, I. Shinohara, M. Fujimoto, A. Matsuoka, Y. Saito, T. Mukai, Construction of magnetic reconnection in the near-Earth magnetotail with geotail. *J. Geophys. Res.* **116**, 4222 (2011). doi:[10.1029/2010JA016283](https://doi.org/10.1029/2010JA016283)
- T. Nagai, S. Zenitani, I. Shinohara, R. Nakamura, M. Fujimoto, Y. Saito, T. Mukai, Ion and electron dynamics in the ion-electron decoupling region of magnetic reconnection with Geotail observations. *J. Geophys. Res. Space Phys.* **118**, 7703–7713 (2013). doi:[10.1002/2013JA019135](https://doi.org/10.1002/2013JA019135)
- R. Nakamura et al., Motion of the dipolarization front during a flow burst event observed by cluster. *Geophys. Res. Lett.* **29**, 1942 (2002). doi:[10.1029/2002GL015763](https://doi.org/10.1029/2002GL015763)
- M. Oieroset, T.D. Phan, M. Fujimoto, R.P. Lin, R.P. Lepping, In situ detection of collisionless reconnection in the Earth's magnetotail. *Nature* **412**, 414–417 (2001). doi:[10.1038/35086520](https://doi.org/10.1038/35086520)
- M. Oieroset, T.D. Phan, J.P. Eastwood, M. Fujimoto, W. Daughton, M.A. Shay, V. Angelopoulos, F.S. Mozer, J.P. McFadden, D.E. Larson, K.-H. Glassmeier, Direct evidence for a three-dimensional magnetic flux rope flanked by two active magnetic reconnection X lines at Earth's magnetopause. *Phys. Rev. Lett.* **107**(16), 165007 (2011). doi:[10.1103/PhysRevLett.107.165007](https://doi.org/10.1103/PhysRevLett.107.165007)
- M. Oka, T.-D. Phan, J.P. Eastwood, V. Angelopoulos, N.A. Murphy, M. Oieroset, Y. Miyashita, M. Fujimoto, J. McFadden, D. Larson, Magnetic reconnection X-line retreat associated with dipolarization of the Earth's magnetosphere. *Geophys. Res. Lett.* **38**, L20105 (2011). doi:[10.1029/2011GL049350](https://doi.org/10.1029/2011GL049350)
- T.D. Phan, B.U.Ö. Sonnerup, R.P. Lin, Fluid and kinetics signatures of reconnection at the dawn tail magnetopause: wind observations. *J. Geophys. Res.* **106**, 25489 (2001). doi:[10.1029/2001JA900054](https://doi.org/10.1029/2001JA900054)
- T.D. Phan, H.U. Frey, S. Frey, L. Peticolas, S. Fuselier, C. Carlson, H. Rème, J.-M. Bosqued, A. Balogh, M. Dunlop, L. Kistler, C. Mouikis, I. Dandouras, J.-A. Sauvaud, S. Mende, J. McFadden, G. Parks, E. Moebius, B. Klecker, G. Paschmann, M. Fujimoto, S. Petrinec, M.F. Marcucci, A. Korth, R. Lundin, Simultaneous cluster and IMAGE observations of cusp reconnection and auroral proton spot for northward IMF. *Geophys. Res. Lett.* **30**, 116 (2003). doi:[10.1029/2003GL016885](https://doi.org/10.1029/2003GL016885)
- T.D. Phan, J.F. Drake, M.A. Shay, F.S. Mozer, J.P. Eastwood, Evidence for an elongated electron diffusion region during fast magnetic reconnection. *Phys. Rev. Lett.* **99**(25), 255002 (2007). doi:[10.1103/PhysRevLett.99.255002](https://doi.org/10.1103/PhysRevLett.99.255002)
- T.D. Phan, G. Paschmann, J.T. Gosling, M. Oieroset, M. Fujimoto, J.F. Drake, V. Angelopoulos, The dependence of magnetic reconnection on plasma β and magnetic shear: evidence from magnetopause observations. *Geophys. Res. Lett.* **40**, 11 (2013). doi:[10.1029/2012GL054528](https://doi.org/10.1029/2012GL054528)
- A. Raj, T. Phan, R.P. Lin, V. Angelopoulos, Wind survey of high-speed bulk flows and field-aligned beams in the near-Earth plasma sheet. *J. Geophys. Res.* **107**, 1419 (2002). doi:[10.1029/2001JA007547](https://doi.org/10.1029/2001JA007547)
- A. Retinò, M.B. Bavassano Cattaneo, M.F. Marcucci, A. Vaivads, M. André, Y. Khotyaintsev, T. Phan, G. Pallocchia, H. Rème, E. Möbius, B. Klecker, C.W. Carlson, M. McCarthy, A. Korth, R. Lundin, A. Balogh, Cluster multispacecraft observations at the high-latitude duskside magnetopause: implication for continuous and component magnetic reconnection. *Ann. Geophys.* **23**, 461–473 (2005). doi:[10.5194/angeo-23-461-2005](https://doi.org/10.5194/angeo-23-461-2005)
- A. Runov, V. Angelopoulos, M.I. Sitnov, V.A. Sergeev, J. Bonnell, J.P. McFadden, D. Larson, K.-H. Glassmeier, U. Auster, THEMIS observations of an earthward-propagating dipolarization front. *Geophys. Res. Lett.* **36**, 14106 (2009). doi:[10.1029/2009GL038980](https://doi.org/10.1029/2009GL038980)
- A. Runov, R. Nakamura, W. Baumjohann, R.A. Treumann, T.L. Zhang, M. Volwerk, Z. Vörös, A. Balogh, K.-H. Glassmeier, B. Klecker, H. Rème, L. Kistler, Current sheet structure near magnetic X-line observed by cluster. *Geophys. Res. Lett.* **30**(11), 110000-1 (2003). doi:[10.1029/2002GL016730](https://doi.org/10.1029/2002GL016730)
- Y. Saito, T. Mukai, T. Terasawa, Kinetic structure of the slow-mode shocks in the Earth's magnetotail, in *New Perspectives on the Earth's Magnetotail*, ed. by A. Nishida, D.N. Baker, S.W.H. Cowley (1998), p. 103
- J.D. Scudder, R.D. Holdaway, W.S. Daughton, H. Karimabadi, V. Roytershteyn, C.T. Russell, J.Y. Lopez, First resolved observations of the demagnetized electron-diffusion region of an astrophysical magnetized reconnection site. *Phys. Rev. Lett.* **108**(22), 225005 (2012). doi:[10.1103/PhysRevLett.108.225005](https://doi.org/10.1103/PhysRevLett.108.225005)
- M.A. Shay, J.F. Drake, The role of electron dissipation on the rate of collisionless magnetic reconnection. *Geophys. Res. Lett.* **25**, 3759–3762 (1998). doi:[10.1029/1998GL900036](https://doi.org/10.1029/1998GL900036)
- M.A. Shay, J.F. Drake, R.E. Denton, D. Biskamp, Structure of the dissipation region during collisionless magnetic reconnection. *J. Geophys. Res.* **103**, 9165–9176 (1998). doi:[10.1029/97JA03528](https://doi.org/10.1029/97JA03528)

- M.A. Shay, J.F. Drake, B.N. Rogers, R.E. Denton, The scaling of collisionless, magnetic reconnection for large systems. *Geophys. Res. Lett.* **26**, 2163 (1999). doi:[10.1029/1999GL900481](https://doi.org/10.1029/1999GL900481)
- M.A. Shay, J.F. Drake, M. Swisdak, Two-scale structure of the electron dissipation region during collisionless magnetic reconnection. *Phys. Rev. Lett.* **99**(15), 155002 (2007). doi:[10.1103/PhysRevLett.99.155002](https://doi.org/10.1103/PhysRevLett.99.155002)
- M.A. Shay, J.F. Drake, J.P. Eastwood, T.D. Phan, Super Alfvénic propagation of reconnection signatures and Poynting flux during substorms. *Phys. Rev. Lett.* **107**, 065001 (2011)
- B.U.Ö. Sonnerup, Magnetic field reconnection, in *Solar System Plasma Processes*, vol. 3, ed. by L.J. Lanzerotti, C.F. Kennel, E.N. Parker (North-Holland, Washington, 1979), p. 45
- B.U.Ö. Sonnerup, G. Paschmann, I. Papamastorakis, N. Sckopke, G. Haerendel, S.J. Bame, J.R. Asbridge, J.T. Gosling, C.T. Russell, Evidence for magnetic field reconnection at the Earth's magnetopause. *J. Geophys. Res.* **86**, 10049–10067 (1981). doi:[10.1029/JA086iA12p10049](https://doi.org/10.1029/JA086iA12p10049)
- M. Swisdak, J.F. Drake, M.A. Shay, J.G. McIlhargey, Transition from antiparallel to component magnetic reconnection. *J. Geophys. Res.* **110**, 5210 (2005). doi:[10.1029/2004JA010748](https://doi.org/10.1029/2004JA010748)
- K.G. Tanaka, A. Retinò, Y. Asano, M. Fujimoto, I. Shinohara, A. Vaivads, Y. Khotyaintsev, M. André, M.B. Bavassano-Cattaneo, S.C. Buchert, C.J. Owen, Effects on magnetic reconnection of a density asymmetry across the current sheet. *Ann. Geophys.* **26**(8), 2471 (2008). doi:[10.5194/angeo-26-2471-2008](https://doi.org/10.5194/angeo-26-2471-2008)
- J.R. Wygant, C.A. Cattell, R. Lysak, Y. Song, J. Dombeck, J. McFadden, F.S. Mozer, C.W. Carlson, G. Parks, E.A. Lucek, A. Balogh, M. Andre, H. Reme, M. Hesse, C. Mouikis, Cluster observations of an intense normal component of the electric field at a thin reconnecting current sheet in the tail and its role in the shock-like acceleration of the ion fluid into the separatrix region. *J. Geophys. Res.* **110**, 9206 (2005). doi:[10.1029/2004JA010708](https://doi.org/10.1029/2004JA010708)
- S. Zenitani, I. Shinohara, T. Nagai, Evidence for the dissipation region in magnetotail reconnection. *Geophys. Res. Lett.* **39**, 11102 (2012). doi:[10.1029/2012GL051938](https://doi.org/10.1029/2012GL051938)
- X.-Z. Zhou, V. Angelopoulos, A. Runov, J. Liu, Y.S. Ge, Emergence of the active magnetotail plasma sheet boundary from transient, localized ion acceleration. *J. Geophys. Res.* **117**, A10216 (2012). doi:[10.1029/2012JA018171](https://doi.org/10.1029/2012JA018171)